Results in Chemistry 23 (2026) 103145

Contents lists available at ScienceDirect

Results in Chemistry

journal homepage: www.sciencedirect.com/journal/results-in-chemistry

Optimization of Azaspirooxindolinone-based PROTACs targeting BTK: Synthesis, kinase profiling, and degradation analysis

Naveen Kumar Rampeesa [a,b], Rambabu Gundla [a,*], Soňa Gurská [c,d], Sabitha Yadam [e], Sudhakar Tangallapalli [a], Sreenivasa Reddy Anugu [b], Juan Bautista De Sanctis [c,d], Petr Džubák [c,d], Marián Hajdúch [c,d], Naresh Kumar Katari [f,g,*], Viswanath Das [c,d,*], Sreekantha Babu Jonnalagadda [f]

[a] Department of Chemistry, School of Science, GITAM University, Hyderabad, 502102, Telangana, India
[b] Aragen Life Sciences Ltd, Medicinal Chemistry Laboratory Division, Hyderabad 500076, India
[c] Institute of Molecular and Translational Medicine, Faculty of Medicine and Dentistry, Palacký University and University Hospital Olomouc, Hněvotínská 1333/5, 779 00 Olomouc, Czech Republic
[d] Institute of Molecular and Translational Medicine, Czech Advanced Technologies and Research Institute, Palacký University Olomouc, Křížkovského 511/8, 77900 Olomouc, Czech Republic
[e] Ciencia Labs LLP, Sadarpatel Nagar, Nizampet X Roads, Hyderanad 500090, Telangana, India
[f] School of Chemistry & Physics, College of Agriculture, Engineering & Science, Westville Campus, University of KwaZulu-Natal, P Bag X 54001, Durban, 4000, South Africa
[g] A&B Laboratories (An AmSpec Group of company), 10100 East Freeway, Suite 100, Houston, TX 77029, USA.

ARTICLE INFO

Keywords:
Azaspirooxindolinone
BTK degradation
Bruton's tyrosine kinase
Kinase inhibition
Linker optimization
PROTAC
Structure–activity relationship

ABSTRACT

Proteolysis-targeting chimeras (PROTACs) are a promising therapeutic modality for targeted protein degradation. Building upon our previous work on azaspirooxindolinone-based scaffolds, we synthesized a new series of BTK-targeting PROTACs using thalidomide as the CRBN-recruiting ligand. Among these, the lead compound — an azaspirooxindolinone-thalidomide conjugate with a two-methylene linker — exhibited the most potent antiproliferative activity against BTK-high RAMOS cells (IC_{50} = 4.19 ± 0.84 μM), with minimal cytotoxicity in non-cancerous fibroblasts. Molecular docking confirmed strong binding to both wild-type BTK (−10.1 kcal/mol) and the C481S mutant (−11.5 kcal/mol), and biochemical validation confirmed BTK inhibition and dose-dependent degradation. A 24 h treatment resulted in a DC_{50} of 3.35 μM and Dmax of ~96% in RAMOS cells. These findings support the further development of this optimized PROTAC as a candidate BTK degrader for treating B-cell malignancies.

1. Introduction

Bruton's tyrosine kinase (BTK) is a non-receptor tyrosine kinase that plays a central role in the signaling pathways of B-cell receptors (BCRs), which are essential for the development, activation, and survival of B cells. Aberrant activation and overexpression of BTK are commonly associated with various hematologic malignancies, including Waldenström's Macroglobulinemia (WM), Mantle Cell Lymphoma (MCL), and Chronic Lymphocytic Leukemia (CLL) [1]. In these diseases, constitutive BTK signaling promotes the proliferation, migration, and survival of malignant B cells, making it a well-validated therapeutic target [2].

Several BTK inhibitors have been developed and approved for the treatment of B-cell malignancies, with ibrutinib being the most prominent example. Ibrutinib exerts its activity through irreversible covalent binding to the cysteine residue at position 481 (Cys481) within the ATP-binding pocket of BTK, thereby suppressing kinase activity and downstream BCR signaling. However, acquired resistance has emerged as a major clinical limitation, most notably due to the Cys481Ser (C481S) mutation, which disrupts covalent binding by irreversible inhibitors such as ibrutinib, leading to reduced clinical responses and disease progression in mantle cell lymphoma and chronic lymphocytic leukemia [3]. Although next-generation reversible BTK inhibitors have been developed to bypass this mutation, additional mutations (e.g., T474I,

* Corresponding authors.
E-mail addresses: rgundla@gitam.edu (R. Gundla), viswanath.das@upol.cz (V. Das).

https://doi.org/10.1016/j.rechem.2026.103145
Received 25 October 2025; Accepted 16 February 2026
Available online 19 February 2026

L528W) and downstream alterations in PLCγ2 can still confer resistance, highlighting the need for alternative approaches [4,5].

Proteolysis-targeting chimeras (PROTACs) have therefore emerged as an alternative therapeutic strategy to address both kinase-dependent and kinase-independent mechanisms of resistance. Unlike conventional ATP-competitive inhibitors, BTK-directed PROTACs promote ubiquitination and proteasomal degradation of the entire BTK protein, enabling the elimination of both wild-type and mutant forms, including C481S variants [4]. Notably, several BTK degraders, such as BGB-16673 and NX-2127, have demonstrated robust degradation of mutant BTK (Fig. 1a) and sustained suppression of downstream signaling in preclinical models and early clinical studies [4,5]. By removing the BTK protein rather than merely inhibiting its catalytic activity, PROTACs also abrogate the non-enzymatic scaffolding functions of BTK, providing a mechanistic advantage under conditions where signaling persists despite kinase inhibition. These features position BTK-targeting PROTACs as a promising next-generation approach for overcoming mutation-driven resistance in B-cell malignancies.

In this study, we focused on the development of BTK-targeting PROTACs using azaspirooxindolinone as the warhead scaffold. Spiroindole derivatives, including spirocyclic oxindoles, are well-known for their rigid three-dimensional structures and broad pharmacological activities, especially their relevance in anticancer drug development [6]. Prior studies have demonstrated their cytotoxic effects across various cancer cell lines, including Huh7, MCF7, and HCT116 [7]. These compounds inhibit tumor cell proliferation and promote apoptosis, often with minimal toxicity to normal cells [8]. Spirooxindole derivatives bearing triazole and thiadiazine moieties have been reported to exhibit strong antitumor activity in multiple cell lines [9].

Building on our earlier work, we previously demonstrated that azaspirooxindolinone-based PROTACs can effectively degrade BTK and suppress downstream signaling pathways in lymphoma models [10]. Notably, one lead compound (PROTAC 7) inhibited phosphorylation of BTK at Tyr233 and Tyr551 and blocked p38 MAPK activation following stimulation. These promising findings prompted further structural optimization to improve potency and selectivity, particularly by modifying linker composition and orientation.

This study aims to expand upon these initial results by synthesizing a new series of azaspirooxindolinone-based PROTACs with varied linker structures. We hypothesize that differences in linker length, flexibility, and chemical functionality will critically influence BTK binding, degradation efficiency, and cellular selectivity. To test this, we performed molecular docking studies and evaluated cytotoxicity across a panel of cancer cell lines, including BTK-expressing models. Our goal was to identify structural features that enhance the efficacy and selectivity of BTK-targeted PROTACs, thereby informing the design of next-generation PROTACs.

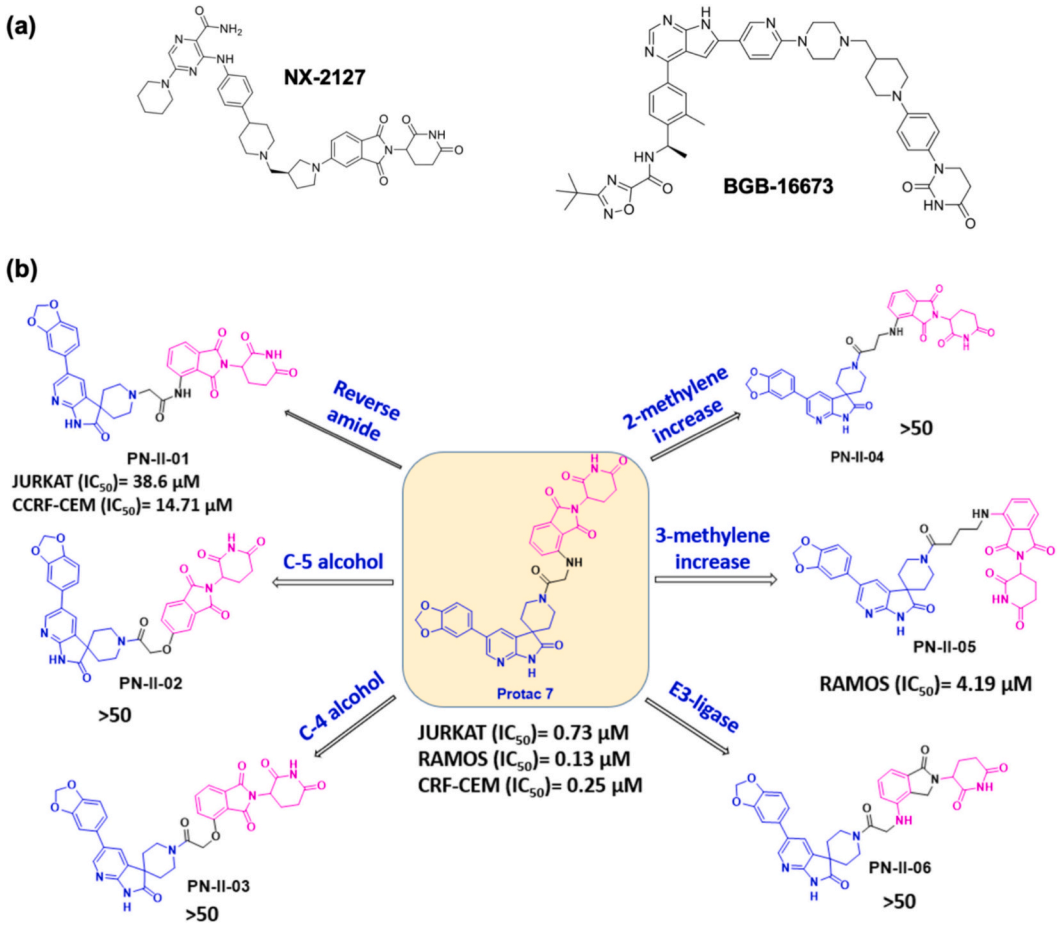

Fig. 1. Clinical BTK PROTACs and rational design of azaspirooxindolinone-based BTK degraders. (**a**) Chemical structures of BTK-targeting PROTACs currently in clinical trials: NX-2127 and BGB-16673. (**b**) Schematic design strategy of azaspirooxindolinone-based PROTACs. The parent compound (PROTAC **7**), which previously demonstrated cytotoxic activity in BTK-expressing Ramos lymphoma cells, was used as a scaffold. Thalidomide (CRBN-binding ligand) and azaspirooxindolinone (BTK warhead) are highlighted in magenta and blue, respectively. (For interpretation of the references to colour in this figure legend, the reader is referred to the web version of this article.)

2. Results and discussion

2.1. Chemistry

Our previous work demonstrated that azaspirooxindolinone-based PROTACs potently degrade BTK in lymphoma cells [10]. However, the impact of structural modifications, such as linker length, linker positioning, and the choice of E3 ligase, on their biological activity remains unexplored. To address this gap, we designed and synthesized a new series of derivatives based on the highly active compound PROTAC 7, aiming to optimize anti-cancer efficacy (Fig. 1b).

We synthesized six new azaspirooxindolinone-based PROTAC compounds by systematically modifying the reported PROTAC **7**. These modifications included elongation of linker length, incorporation of alcohol and reverse amide functionalities, and substitution of the E3 ligase. The resulting compounds were evaluated for cytotoxic activity across a panel of cancer cell lines, with particular focus on BTK-high models. Six compounds were created: two compounds with extended methylene linkers (**PN-II-04 and PN-II-05)**, one with a reverse amide change (**PN-II-01**), two alcohol variants (C-4 is **PN-II-03** and C-5 is **PN-II-02**), and one incorporating a different E3 ligase (**PN-II-06**).

Docking studies were used to guide the design process. These identified solvent-exposed regions within the BTK binding pocket interact with the azaspirooxindolinone scaffold, offering suitable positions for linker attachment. Based on this, PROTACs **PN-II-01** to **PN-II-06** were constructed by linking the azaspirooxindolinone core to thalidomide using structurally diverse linkers, including reverse amide, C-5 alcohol, C-4 alcohol, and two- or three-methylene spacers. These structural variations were designed to assess how linker orientation and flexibility affect the engagement of BTK and the recruitment of the E3 ligase.

2.2. Evaluation of anti-Cancer activity

The cytotoxic effects of the six synthesized BTK-targeting PROTACs were evaluated across a panel of BTK-expressing cancer cell lines and non-cancerous fibroblasts. The cancer panel included colorectal (HCT116, HCT116 p53), lung (A549), osteosarcoma (U2OS), T-cell (Jurkat, CCRF-CEM), B-cell (RAMOS), and myeloid (K562) models. Non-cancerous controls included lung- and foreskin-derived fibroblasts (MRC-5, BJ). BTK-expressing cell lines, RAMOS and K562, express wild-type BTK.

Among the compounds tested, **PN-II-05** showed the strongest anti-proliferative effect in RAMOS cells, with an IC_{50} of 4.19 ± 0.84 μM (Table 1), and minimal toxicity in non-cancerous cells, indicating favorable selectivity towards BTK-high cancer cells. While previous studies did not directly evaluate selectivity, several BTK-targeting agents have demonstrated cytotoxicity in lymphoid malignancies through mechanisms involving cytokine suppression, cell cycle arrest, and BTK degradation. PROTACs based on thalidomide conjugation have also shown effective BTK degradation via CRBN- and proteasome-dependent pathways [11–13,16].

Extension of the linker by a single methylene unit in **PN-II-04** abolished activity in BTK-high RAMOS cells, whereas the two-methylene linker in **PN-II-05** markedly enhanced cytotoxicity (Table 1). Alcohol-functionalized analogues **PN-II-02** (C-5) and **PN-II-03** (C-4) were inactive, suggesting polar modifications at these sites are not compatible with BTK engagement. The reverse amide compound **PN-II-01** showed moderate activity in ITK-high cells but lacked efficacy in BTK-driven lines, indicating altered selectivity. In contrast, **PN-II-06**, which features a substituted E3 ligase, was inactive across all tested cell lines, suggesting that the choice of E3 ligase plays a critical role in mediating BTK degradation and associated cytotoxicity. These findings highlight the importance of linker composition and E3 ligase selection in determining the potency and specificity of BTK-targeted degraders.

2.3. Molecular docking analysis of PN-II-05 binding to BTK and C481S mutant BTK

To better understand the molecular interactions contributing to the cytotoxicity of **PN-II-05** in BTK-high RAMOS cells, molecular docking studies were performed using both wild-type BTK and the clinically relevant C481S mutant. **PN-II-05** exhibited strong binding affinity to wild-type BTK, with a predicted binding energy of −10.1 kcal/mol **(**Fig. 2A**),** and even greater affinity to the C481S mutant, with a docking score of −11.5 kcal/mol **(**Fig. 2B**).** This suggests that **PN-II-05** can accommodate the structural changes induced by the Cys481Ser mutation, which is associated with resistance to covalent inhibitors, such as ibrutinib.

Interaction maps revealed that **PN-II-05** forms hydrogen bonds with critical residues, such as VAL355 and ASP420, in the wild-type protein and maintains favorable contacts in the mutant as well (Fig. 2, right panel). These docking results highlight **PN-II-05** as a mutation-tolerant BTK binder, supporting its potential to engage both wild-type and C481S mutant forms of BTK.

2.4. Functional validation of PN-II-05 through BTK inhibition and degradation

To assess the functional activity of **PN-II-05**, we performed in vitro kinase assays using recombinant BTK and ITK enzymes. **PN-II-05** selectively inhibited BTK in a dose-dependent manner, whereas ITK activity remained unaffected up to 10 μM (Fig. 3a, b). Ibrutinib (100 nM) was included as a positive control to validate assay performance, based on prior dose–response data showing >75% inhibition at this concentration [10] (see Supplementary **Fig. S1**).

To evaluate BTK degradation, RAMOS cells were treated with PN-II-05 (0–10 μM) for 24 h, and BTK protein levels were measured by Western blot. Quantification revealed dose-dependent degradation, which was fitted to a four-parameter logistic (4PL) regression model. The analysis yielded a half-degradation concentration (DC_{50}) of 3.35 μM, with a maximum degradation (Dmax) of approximately 96% (Fig. 3c, d). These findings confirm the PROTAC mechanism of PN-II-05 and support its potential as an effective BTK degrader.

Table 1
Cytotoxic activity (IC_{50}, μM) of synthesized PROTACs across cancerous and non-cancerous cell lines. Values are reported as mean ± SD from at least six replicates ($n \geq 6$). RAMOS cells represent BTK (wildtype)-high models, while Jurkat cells represent ITK-high models.

PROTAC	BTK null				ITK positive		BTK positive		Non-cancer	
	A549	**HCT116**	**HCT116 p53$^{-/-}$**	**U2OS**	**Jurkat**	**CCRF-CEM**	**RAMOS**	**K562**	**MRC-5**	**BJ**
PN-II-01	>50	>50	>50	>50	37.6 ± 7.02	14.71	>50	>50	>50	>50
PN-II-02	>50	>50	>50	>50	>50	>50	>50	>50	>50	>50
PN-II-03	>50	>50	>50	>50	>50	>50	>50	>50	>50	>50
PN-II-04	>50	>50	>50	>50	>50	>50	>50	>50	>50	>50
PN-II-05	>50	>50	>50	>50	>50	>50	4.19 ± 0.84	>50	>50	>50
PN-II-06	>50	>50	>50	>50	>50	>50	>50	>50	>50	>50

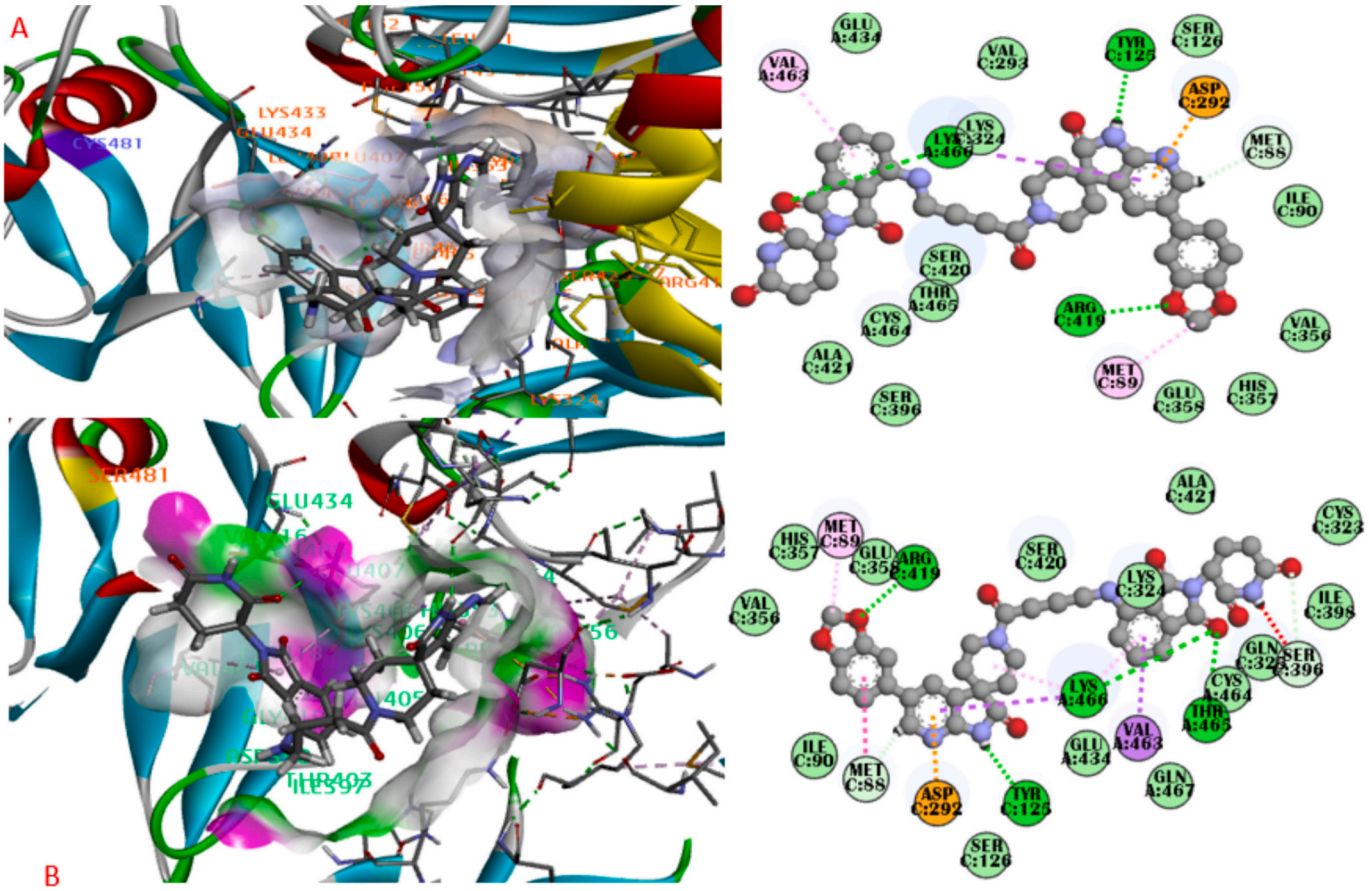

Fig. 2. Predicted binding modes of PN-II-05 with wild-type BTK and the C481S mutant. (A) 3D docking pose of PN-II-05 within the ATP-binding cleft of wild-type BTK. (B) 3D docking pose of PN-II-05 within the ATP-binding cleft of C481S mutant BTK. (Right) 2D ligand interaction map highlighting key active-site residues involved in PN-II-05 binding. All docking scores and associated interaction data are provided in the Supplementary Information.

3. Conclusion

This study highlights the rational design and synthesis of azaspirooxindolinone-based PROTACs targeting BTK, with **PN-II-05** emerging as a promising compound. **PN-II-05** exhibited potent cytotoxicity in BTK-high RAMOS cells and demonstrated a favorable safety profile in non-cancerous cells. Functional assays confirmed its kinase inhibition and degradation activity, with a DC_{50} of 3.35 μM and a Dmax of ~96%. Molecular docking revealed strong binding to both wild-type and C481S mutant BTK, suggesting potential relevance for overcoming resistance mutations. While the C481S interaction was evaluated at the molecular docking level, experimental validation in mutation-bearing cellular models remains an important objective for future studies. These findings provide a structural and functional rationale for advancing **PN-II-05** as a candidate BTK-targeting degrader, warranting further studies to assess kinase-family selectivity and therapeutic potential. Further studies, including in vivo pharmacokinetics and efficacy evaluation, are needed to confirm the therapeutic potential of **PN-II-05** and support its advancement as a BTK-targeting degrader.

4. Experimental section

4.1. Materials and physical measurements

All chemicals were purchased from Lancaster (Alfa Aesar, Johnson Matthey Co., Ward Hill, MA, USA), Sigma-Aldrich (St. Louis, MO, USA), and Spectrochem Pvt. Ltd. (Mumbai, India). Amino acids and their esters were obtained from Combi-Blocks, Inc. (San Diego, USA) and BLD Pharm (India). Reactions were monitored by thin-layer chromatography (TLC) on aluminum-backed silica gel plates (F254S), and visualized under UV light or by $KMnO_4$ and iodine staining.

^1H and ^{13}C NMR spectra were recorded on a Bruker 400 MHz spectrometer (Billerica, MA, USA), with chemical shifts reported in ppm downfield from TMS. Signal patterns are abbreviated as s (singlet), d (doublet), dd (double doublet), t (triplet), td (triplet of a doublet), bs (broad singlet), and m (multiplet). ESI mass spectra were acquired using a Micromass Quattro LC in positive ion mode (ESI^+) with a capillary voltage of 3.98 kV. IR spectra were recorded on an FT-IR spectrometer, with major absorption peaks reported in cm^{-1}. All solutions were prepared in deionized distilled water. Unless otherwise stated, reagents were of analytical grade and used without further purification.

4.2. Chemistry

To synthesize **PN-II-01**, **2** was treated with chloroacetyl chloride (Scheme 1), followed by N-alkylation with **1** (Scheme 3). For **PN-II-02**, tert-butyl bromoacetate was first alkylated with **6**, followed by tert-butyl deprotection (Scheme 1) and coupling with **1** (Scheme 3). **PN-II-03** was synthesized by alkylation of tert-butyl bromoacetate with **9**, followed by deprotection (Scheme 1) and coupling with **1** (Scheme 3). For **PN-II-04**, nucleophilic substitution of **13** with **12** was followed by deprotection (Scheme 2) and coupling with **1** (Scheme 3). **PN-II-05** was obtained by nucleophilic substitution of **16** with **12**, followed by deprotection (Scheme 2) and coupling with **1** (Scheme 3). For **PN-II-06**, tert-butyl bromoacetate was first alkylated with **6**, then deprotected (Scheme 1) and coupled with **1** (Scheme 3).

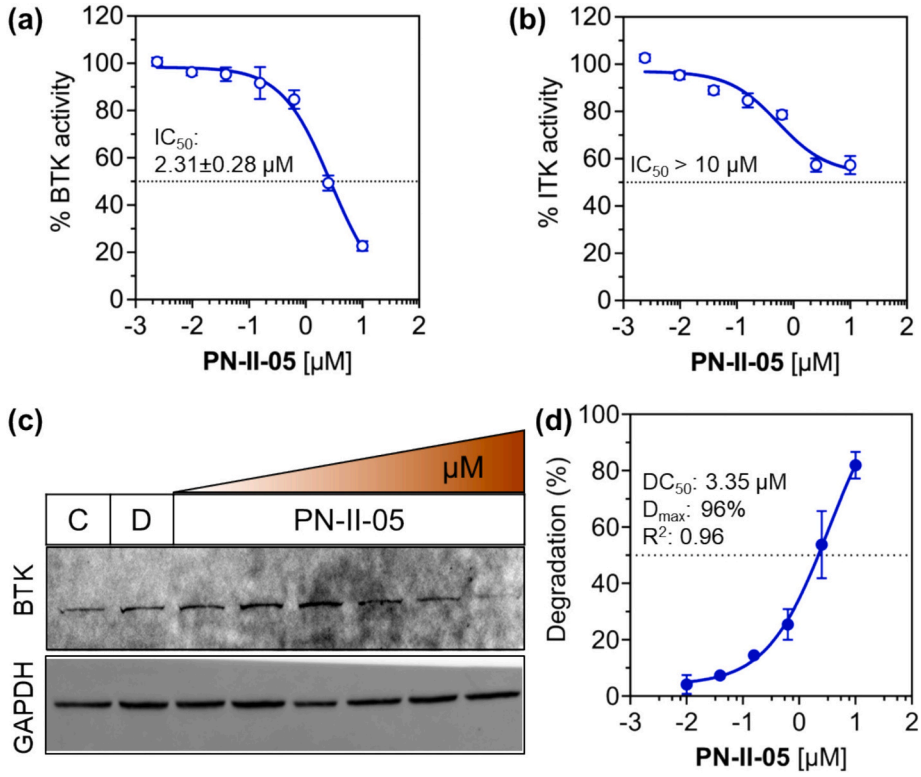

Fig. 3. BTK kinase inhibition and degradation by PN-II-05. (**a, b**) Dose–response inhibition curves of recombinant BTK (a) and ITK (b) by PN-II-05, measured using the ADP-Glo™ Kinase Assay. 2.91 ± 0.29 μM, with no measurable inhibition of ITK up to 10 μM. Mean ± SEM ($n = 3$). (c) Western blot analysis showing dose-dependent degradation of BTK in RAMOS cells treated with PN-II-05 (0–10 μM) for 24 h. GAPDH was used as a loading control. In panel (c), "C" indicates untreated control, and "D" represents vehicle (DMSO) control with a final concentration of 0.1%, equivalent to that in the highest drug-treated sample. Uncropped blots are provided in the supplementary information. (d) Quantification of BTK degradation from panel (c), plotted as the percentage of BTK remaining relative to the DMSO-treated control. Curve fitting performed using 4PL model. Mean ± SEM ($n = 2$).

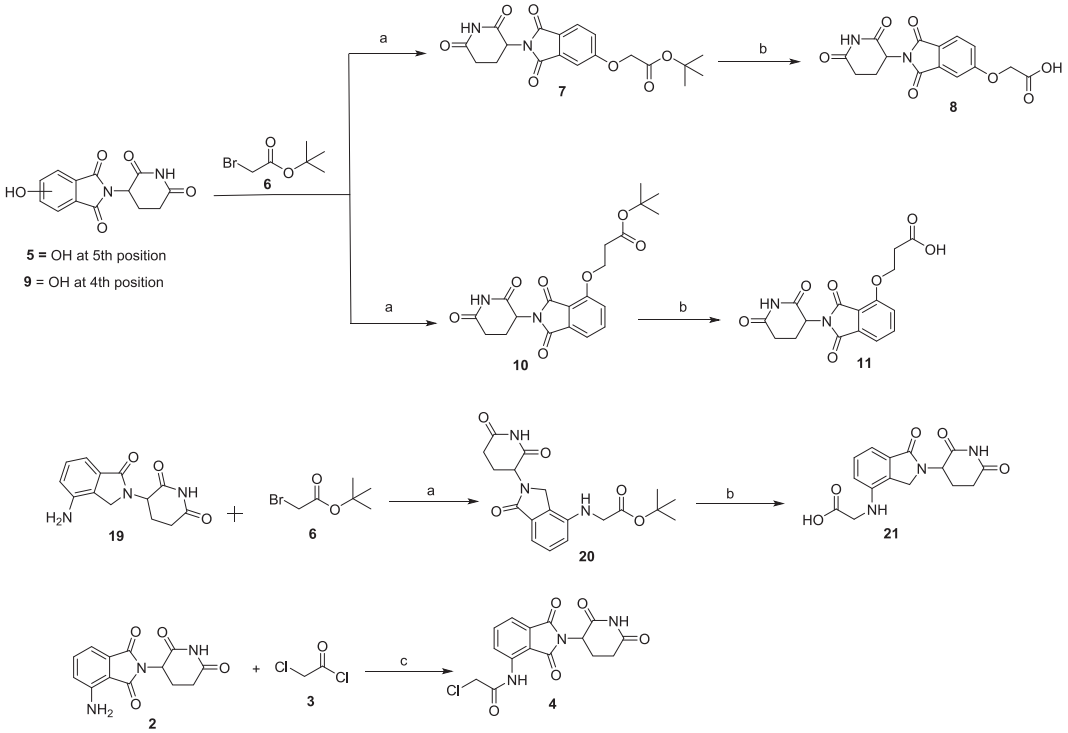

Scheme 1. Reaction conditions: (a) K_2CO_3, DMF, room temperature, 16 h; (b) TFA, DCM, room temperature, 16 h; (c) THF, reflux.

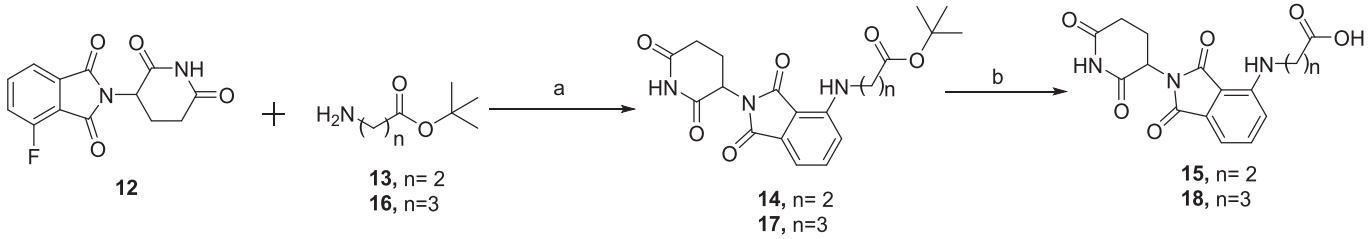

Scheme 2. Reaction conditions: (a) DIPEA, DMSO, 100 °C, 16 h; (b) TFA, DCM, room temperature, 16 h.

4.2.1. General procedure B: De-protection of the tertiary butyl ester group

To a solution of the tert-butyl ester in dry dichloromethane (10 v) at 0 °C, TFA (5 equivalents) was added. The mixture was stirred at room temperature for 16 h. The reaction mixture was monitored by TLC and LC-MS. After completion, the reaction was concentrated under reduced pressure and co-distilled with diethyl ether to yield the TFA salt of the product, which was used directly in the next step without purification.

4.2.1.1. Procedure for 5′-(benzo[d][1,3]dioxol-5-yl)spiro[piperidine-4,3′-pyrrolo[2,3-b]pyridin]-2′(1′H)-one (compound 1). **Compound 1** was prepared using the procedure reported previously [14].

4.2.1.2. Procedure for 2-(2,6-dioxopiperidin-3-yl)-4-fluoroisoindoline-1,3-dione (compound 12). A mixture of 4-fluoroisobenzofuran-1,3-dione (2 g, 12.19 mmol), 3-aminopiperidine-2,6-dione hydrochloride (2.02 g, 12.19 mmol), and NaOAc (1.5 g, 18.29 mmol) in HOAc (20 mL) was stirred at 135 °C for 16 h. The mixture was cooled and concentrated under vacuum. The residue was suspended in water (100 mL) and stirred at room temperature for 2 h. The solid was collected by filtration and dried under vacuum to afford **2-(2,6-dioxopiperidin-3-yl)-4-fluoroisoindoline-1,3-dione (Compound 12)** as a beige solid (3.0 g, 91% yield).

MS (ESI$^+$): m/z = 277.25 (M + H).

Compound 12 was prepared using a reported procedure [15].

Procedure for 2-chloro-N-(2-(2,6-dioxopiperidin-3-yl)-1,3-dioxoisoindolin-4-yl)acetamide (Compound 4)

To a solution of 4-amino-2-(2,6-dioxopiperidin-3-yl)isoindoline-1,3-dione (**2**) (50 mg, 0.183 mmol, 1.0 equiv.) and chloroacetyl chloride (22.5 mg, 0.201 mmol, 1.1 equiv.) in THF (1 mL), the mixture was stirred at reflux for 16 h and monitored by TLC and LC-MS. After completion, the reaction mixture was cooled, and the resulting solid was filtered, washed with THF (1 mL), and dried under vacuum to afford 2-chloro-N-(2-(2,6-dioxopiperidin-3-yl)-1,3-dioxoisoindolin-4-yl)acetamide **(4)** (40 mg, 63%) as an off-white solid. This crude product was used directly in the next step without purification [16].

Preparation of 2-(5′-(benzo[d] [1,3] dioxol-5-yl)-2′-oxo-1′,2′-dihydrospiro [piperidine-4,3′-pyrrolo [2,3-*b*] pyridin] -1-yl)-N-(2-(2,6-dioxopiperidin-3-yl)-1,3-dioxoisoindolin-4-yl)acetamide (PN-II-01).

To a stirred solution of **4** (45 mg, 0.128 mmol, 1.0 equiv.) and **1** (41 mg, 0.128 mmol, 1.0 equiv.) in DMF (0.5 mL), potassium carbonate (26 mg, 0.19 mmol, 1.5 equiv.) was added at room temperature. The heterogeneous reaction mixture was stirred at room temperature for 16 h and monitored by TLC and LC-MS. After completion, the reaction was diluted with water (2 mL) and extracted with ethyl acetate (2 × 10 mL). The organic layer was washed with water and brine, dried over sodium sulfate, filtered, and concentrated under reduced pressure to yield the crude product.

Purification was performed by flash chromatography on 12 g silica gel (REVELERIS), eluting with 2–4% methanol in dichloromethane, followed by two rounds of GRACE C18 reverse-phase purification using 12 g cartridges and 35–40% acetonitrile/0.05% formic acid in water. The purified fractions were lyophilized to afford **PN-II-01** (11 mg, 12%) as a pale-yellow solid.

^{1}H NMR (400 MHz, $CDCl_3$ + MeOD): δ 8.90 (d, 1H), 8.21 (s, 1H), 7.87 (s, 1H), 7.75 (t, 1H), 7.58 (d, 1H), 7.01–6.98 (m, 3H), 6.91 (d, 1H), 6.03 (d, 1H), 4.89–4.85 (m, 1H), 3.24–3.19 (m, 2H), 2.86–2.73 (m, 5H), 2.55–2.45 (m, 2H), 2.22–2.06 (m, 6H), 1.27–1.23 (m, 2H). **^{13}C NMR** (400 MHz, DMSO-d_6): δ 181.1, 171.7, 170.9, 168.5, 168.2, 166.9, 154.3, 148.4, 147.5, 144.3, 136.6, 136.2, 132.0, 131.6, 131.3, 130.0, 129.4, 124.9, 120.4, 118.5, 116.0, 108.9, 107.0, 101.5, 61.8, 44.7, 32.6, 30.9, 22.5. **LC-MS (ESI$^+$):** m/z = 637.1 (M + H)$^+$; **IR (neat):** 1635.6 cm^{-1} (C═O stretching); **Melting range:** 225–227 °C.

Preparation of tert-butyl 2-((2-(2,6-dioxopiperidin-3-yl)-1,3-dioxoisoindolin-5-yl)oxy)acetate (Compound 7).

To a stirred solution of 2-(2,6-dioxopiperidin-3-yl)-5-hydroxyisoindoline-1,3-dione **(5)** (500 mg, 1.83 mmol, 1.0 equiv.) and tert-butyl bromoacetate (533 mg, 2.73 mmol, 1.5 equiv.) in DMF (5 mL), potassium carbonate (302 mg, 2.73 mmol, 1.5 equiv.) was added at room temperature. The reaction mixture was stirred at room temperature for 16 h and monitored by TLC and LC-MS. After completion, the reaction was diluted with water (20 mL) and extracted with ethyl acetate (3 × 10 mL). The combined organic layer was washed with water and brine, dried over sodium sulfate, filtered, and concentrated under reduced pressure to obtain the crude product. Purification was performed by GRACE flash chromatography using 12 g silica (REVELERIS), eluting with 30–40% ethyl acetate in petroleum ether to afford **7** (255 mg, 41%) as a pale yellow foamy solid.

^{1}H NMR (400 MHz, $CDCl_3$): δ 7.96 (bs, 1H), 7.80 (d, 1H), 7.30 (d, 1H), 7.23 (dd, 1H), 4.95 (dd, 1H), 4.64 (s, 2H), 2.95–2.72 (m, 3H), 2.17–2.15 (m, 1H), 1.50 (m, 9H).

Preparation of 2-((2-(2,6-dioxopiperidin-3-yl)-1,3-dioxoisoindolin-5-yl)oxy)acetic acid (Compound 8).

Compound 8 was prepared from **7** (50 mg) using General Procedure B. The reaction yielded 50 mg of crude **8** as a pale yellow, viscous liquid, which was used directly in the next step without purification.

Preparation of 5-(2-(5′-(benzo [d] [1,3] dioxol-5-yl)-2′-oxo-1′,2′-dihydrospiro [piperidine-4,3′-pyrrolo [2,3-*b*] pyridin] -1-yl)-2-oxoethoxy)-2-(2,6-dioxopiperidin-3-yl)isoindoline-1,3-dione (PN-II-02).

To a stirred solution of **1** (40 mg, 0.123 mmol) in DMF (0.5 mL) at 0 °C under a nitrogen atmosphere were added **8** (40 mg, 0.123 mmol), HATU (70 mg, 0.184 mmol, 1.5 equiv.), and DIPEA (0.064 mL, 0.369 mmol, 3 equiv.). The reaction mixture was stirred at room temperature for 1 h and monitored by TLC. Upon completion, the mixture was diluted with water (2 mL) and extracted with ethyl acetate (3 × 10 mL). The combined organic layer was washed with brine (2 × 10 mL), dried over sodium sulfate, and concentrated to obtain the crude product. Purification was carried out in two steps using GRACE C18 reverse-phase cartridges (12 g, REVELERIS), eluting with 30–35% acetonitrile/0.05% formic acid in water. The pure fractions were lyophilized to afford **PN-II-02** (21 mg, 27%) as a pale yellow solid. **^{1}H NMR** (400 MHz, DMSO-d_6): δ 11.05 (bs, 2H), 8.35 (s, 1H), 8.12 (s, 1H), 7.85 (d, 1H), 7.42 (s, 1H), 7.40 (d, 1H), 7.32 (s, 1H), 7.18 (d, 1H), 7.03 (d, 1H), 6.06 (s, 1H), 5.25 (d, 1H), 5.17–5.10 (m, 2H), 3.91–3.74 (m, 4H), 2.94–2.85 (m, 1H), 2.62–2.55 (m, 2H), 2.09–2.04 (m, 1H), 1.98–1.76 (m, 4H). **^{13}C NMR** (400 MHz, DMSO-d_6): δ 180.3, 172.7, 169.9, 166.9, 166.7, 165.1, 155.0, 147.9, 146.7, 144.1, 133.7, 131.6, 129.9, 129.5, 128.1, 125.1,

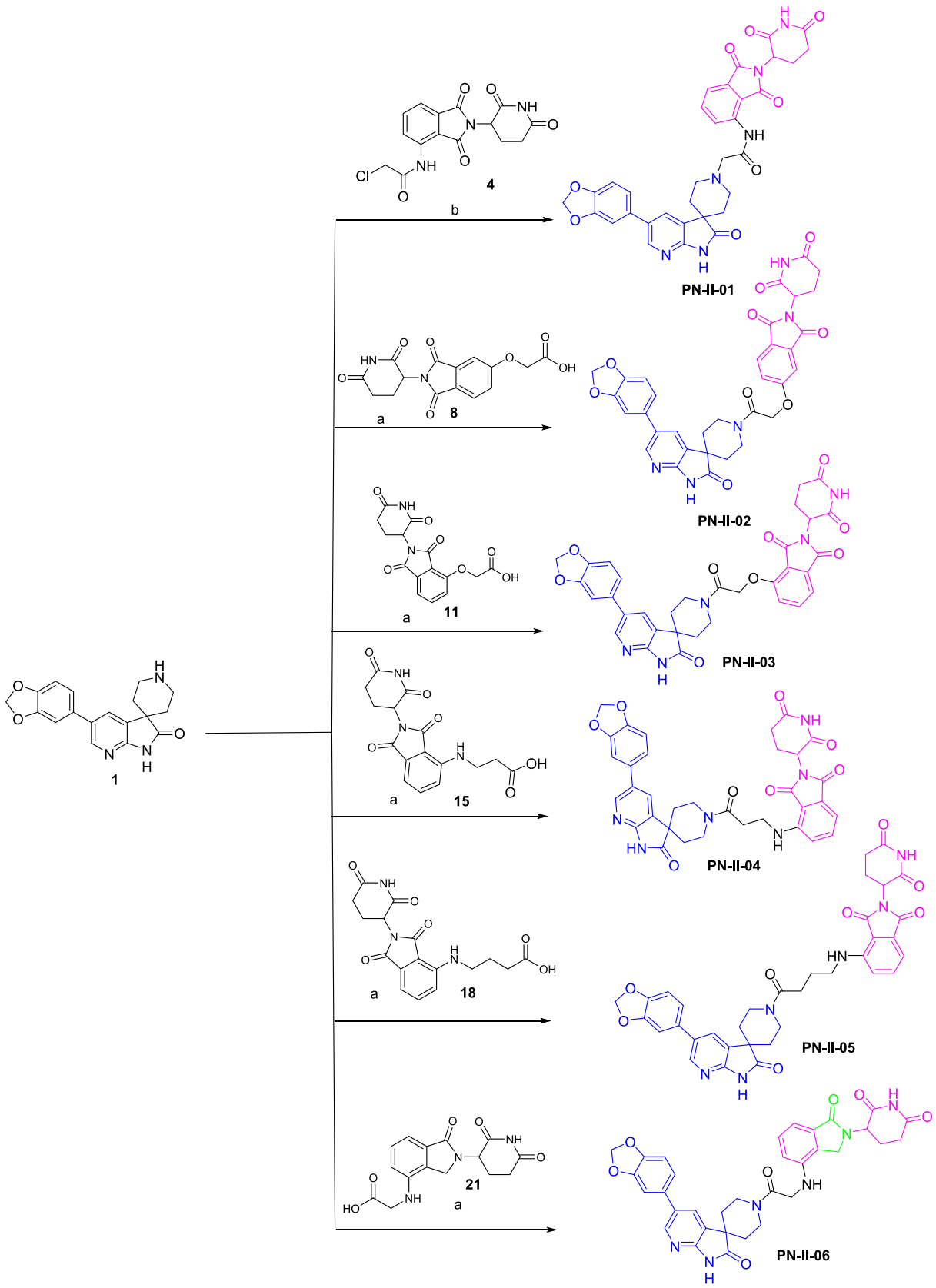

Scheme 3. Reaction conditions: (a) HATU, DIPEA, DMF, room temperature, 1 h; (b) K_2CO_3, DMF, room temperature, 16 h.

123.1, 121.2, 120.0, 109.1, 108.6, 107.0, 101.1, 66.2, 48.9, 45.2, 36.9, 31.7, 31.2, 30.9, 22.0. **LC-MS (ESI$^+$):** m/z = 638.2 (M + H)$^+$; **IR:** 1710 cm^{-1} (C═O stretching); **Melting range:** 162–165 °C.

Preparation of tert-butyl 2-((2-(2,6-dioxopiperidin-3-yl)-1,3-dioxoisoindolin-5-yl)oxy)acetate (Compound 10).

To a stirred solution of 2-(2,6-dioxopiperidin-3-yl)-5-hydroxyisoindoline-1,3-dione **(9)** (500 mg, 1.83 mmol, 1.0 equiv.) and tert-butyl bromoacetate (533 mg, 2.73 mmol, 1.5 equiv.) in DMF (5 mL), potassium carbonate (302 mg, 2.73 mmol, 1.5 equiv.) was added at room temperature. The mixture was stirred for 16 h and monitored by TLC and LC-MS. After completion, the reaction mixture was diluted with water (10 mL) and extracted with ethyl acetate (3 × 20 mL). The organic layer was washed with water and brine, dried over sodium sulfate, filtered, and concentrated under reduced pressure. The crude product was purified by GRACE silica chromatography (24 g, RELEVERIS), eluting with 30–40% ethyl acetate in petroleum ether to afford **10** (270 mg, 40%) as a pale yellow foamy solid. **^{1}H NMR** (400 MHz, $CDCl_3$): δ 7.95 (bs, 1H), 7.67 (t, 1H), 7.51 (d, 1H), 7.11 (dd, 1H), 4.95 (dd, 1H), 4.79 (s, 2H), 2.92–2.73 (m, 3H), 2.15–2.04 (m, 1H), 1.48 (m, 9H).

Preparation of 2-((2-(2,6-dioxopiperidin-3-yl)-1,3-dioxoisoindolin-5-yl)oxy)acetic acid (Compound 11).

Compound 11 was prepared from **10** (50 mg) using General Procedure B. The resulting crude **11** (50 mg) was obtained as a pale-yellow viscous liquid and used directly in the next step without purification [17].

Preparation of 4-(2-(5′-(benzo [d] [1,3] dioxol-5-yl)-2′-oxo-1′,2′-dihydrospiro [piperidine-4,3′-pyrrolo [2,3-*b*] pyridin] -1-yl)-2-oxoethoxy)-2-(2,6-dioxopiperidin-3-yl)isoindoline-1,3-dione (PN-II-03).

To a stirred solution of **1** (40 mg, 0.123 mmol) in DMF (0.5 mL) at 0 °C under nitrogen were added **11** (40 mg, 0.123 mmol), HATU (70 mg, 0.184 mmol, 1.5 equiv.), and DIPEA (0.064 mL, 0.369 mmol, 3 equiv.). The reaction mixture was stirred at room temperature for 1 h and monitored by TLC. After completion, the mixture was diluted with water (5 mL) and extracted with ethyl acetate (3 × 10 mL). The organic phase was washed with brine (2 × 10 mL), dried over sodium sulfate, and concentrated under reduced pressure. The crude product was purified twice using GRACE C18 reverse-phase chromatography (12 g, RELEVERIS), eluting with 30–40% acetonitrile/0.05% formic acid in water. The purified product was lyophilized to afford **PN-II-03** (21 mg, 27%) as a pale yellow solid. **^{1}H NMR** (400 MHz, DMSO-d_6): δ 11.10 (s, 2H), 8.35 (d, 1H), 8.09 (s, 1H), 7.80 (t, 1H), 7.46 (d, 1H), 7.40 (d, 1H), 7.17 (d, 1H), 7.00 (d, 1H), 6.06 (s, 1H), 5.23 (d, 1H), 5.20 (d, 1H), 5.11–5.07 (m, 1H), 3.92–3.78 (m, 4H), 2.91–2.83 (m, 1H), 2.67–2.53 (m, 2H), 2.05–1.77 (m, 5H). **^{13}C NMR** (400 MHz, DMSO-d_6): δ 180.4, 172.7, 169.8, 166.7, 165.2, 165.0, 155.6, 155.0, 148.0, 146.8, 144.1, 136.5, 133.0, 131.6, 129.9, 129.5, 128.1, 120.0, 116.1, 115.4, 108.6, 107.0, 101.1, 66.1, 48.7, 45.1, 36.9, 31.7, 31.2, 30.9, 21.9.

LC-MS (ESI$^+$): m/z = 638.2 (M + H)$^+$; **IR:** 1710 cm^{-1} (C═O stretching); **Melting range:** 178–180 °C.

Preparation of tert-butyl 4-(2-(5′-(benzo [d] [1,3] dioxol-5-yl)-2′-oxo-1′,2′-dihydrospiro [piperidine-4,3′-pyrrolo [2,3-*b*] pyridin] -1-yl)-2-oxoethoxy)-2-(2,6-dioxopiperidin-3-yl)isoindoline-1,3-dione (Compound 14).

To a solution of 2-(2,6-dioxopiperidin-3-yl)-4-fluoroisoindoline-1,3-dione **(12)** (100 mg, 0.36 mmol, 1.0 equiv.) and tert-butyl 3-aminopropanoate **(13)** (28 mg, 0.432 mmol, 1.2 equiv.) in DMSO (1 mL) was added DIPEA (0.18 mL, 1.08 mmol, 3.0 equiv.) at room temperature. The mixture was stirred at 100 °C for 16 h and monitored by TLC and LC-MS. Upon completion, the reaction mixture was cooled, diluted with water (5 mL), and extracted with ethyl acetate (3 × 15 mL). The organic layer was washed with water and brine, dried over sodium sulfate, filtered, and concentrated under reduced pressure. The crude product was purified using GRACE silica gel chromatography (12 g, RELEVERIS), eluting with 40–50% ethyl acetate in petroleum ether, to afford **14** (60 mg, 41%) as a pale yellow foamy solid. **^{1}H NMR** (400 MHz, $CDCl_3$): δ 7.93 (bs, 1H), 7.51 (t, 1H), 7.11 (d, 1H), 6.93 (d, 1H), 6.45 (t, 1H), 4.91 (dd, 1H), 3.56 (q, 2H), 2.91–2.71 (m, 3H), 2.57 (t, 1H), 2.14–2.10 (m, 1H), 1.46 (s, 9H). **LC-MS (ESI$^+$):** m/z = 402.1 (M + H)$^+$.

Preparation of 3-((2-(2,6-dioxopiperidin-3-yl)-1,3-dioxoisoindolin-4-yl)amino)propanoic acid (Compound 15).

Compound 15 was prepared from **14** (60 mg) using General Procedure B. The deprotection yielded **15** (60 mg) as a pale-yellow viscous liquid. This crude product was used directly in the next step without purification [18].

Preparation of4-((3-(5′-(benzo [d] [1,3] dioxol-5-yl)-2′-oxo-1′,2′-dihydrospiro [piperidine-4,3′-pyrrolo [2,3-*b*] pyridin] -1-yl)-3-oxopropyl)amino)-2-(2,6-dioxopiperidin-3-yl)isoindoline-1,3-dione (PN-II-04).

To a stirred solution of **1** (50 mg, 0.154 mmol) in DMF (0.5 mL) at 0 °C under a nitrogen atmosphere, were added **15** (60 mg, 0.184 mmol, 1.2 equiv.), HATU (70 mg, 0.184 mmol, 1.2 equiv.), and DIPEA (0.064 mL, 0.462 mmol, 3 equiv.). The reaction mixture was stirred at room temperature for 1 h and monitored by TLC. After completion, the mixture was diluted with water (5 mL) and extracted with ethyl acetate (3 × 10 mL). The organic layer was washed with brine (2 × 10 mL), dried over sodium sulfate, and concentrated under reduced pressure. The crude product was purified twice by GRACE reverse-phase chromatography (12 g C18, RELEVERIS), eluting with 35–40% acetonitrile/0.05% formic acid in water. The purified fractions were lyophilized to yield **PN-II-04** (25 mg, 25%) as a pale yellow solid. **^{1}H NMR** (400 MHz, DMSO-d_6): δ 11.12 (s, 1H), 11.08 (s, 1H), 8.33 (d, 1H), 8.10 (s, 1H), 7.62–7.58 (m, 1H), 7.32 (d, 1H), 7.18 (dd, 2H), 7.01 (dd, 2H), 6.83 (t, 1H), 6.05 (s, 2H), 5.05–5.01 (m, 1H), 3.85–3.82 (m, 3H), 3.75–3.65 (m, 1H), 3.60–3.59 (m, 2H), 2.91–2.82 (m, 3H), 2.72–2.66 (m, 1H), 2.60–2.59 (m, 1H), 2.03–2.00 (m, 2H), 1.82–1.74 (m, 4H). **^{13}C NMR** (400 MHz, DMSO-d_6): δ 180.3, 172.7, 170.0, 169.2, 168.8, 167.2, 154.9, 155.0, 147.9, 146.7, 146.1, 144.0, 136.3, 132.2, 131.5, 129.8, 129.6, 120.0, 117.0, 115.4, 109.2, 108.6, 107.1, 101.1, 48.5, 45.3, 36.5, 32.0, 31.8, 31.3, 30.9, 22.1. **LC-MS (ESI$^+$):** m/z = 651.2 (M + H)$^+$; **IR:** 1701.2 cm^{-1} (C═O stretching); **Melting range:** 149–151 °C.

Preparation of tert-tert-butyl 4-((2-(2,6-dioxopiperidin-3-yl)-1,3-dioxoisoindolin-4-yl)amino)butanoate (Compound 17).

To a stirred solution of 2-(2,6-dioxopiperidin-3-yl)-4-fluoroisoindoline-1,3-dione **(12)** (500 mg, 1.81 mmol) and tert-butyl 4-aminobutanoate **(16)** (353 mg, 1.81 mmol, 1.0 equiv.) in DMSO (5 mL), DIPEA (1.6 mL, 9.05 mmol, 5.0 equiv.) was added at room temperature. The mixture was stirred at 100 °C for 16 h and monitored by TLC and LC-MS. After completion, the reaction mixture was cooled, diluted with water (10 mL), and extracted with ethyl acetate (3 × 10 mL). The combined organic phase was washed with water and brine, dried over sodium sulfate, and concentrated under reduced pressure. The crude product was purified by GRACE normal-phase chromatography (12 g, RELEVERIS), eluting with 50–55% ethyl acetate in petroleum ether, to afford **17** (200 mg, 27%) as a yellow solid. **^{1}H NMR** (400 MHz, $CDCl_3$): δ 7.99 (bs, 1H), 7.50 (t, 1H), 7.10 (d, 1H), 6.93 (d, 1H), 6.29 (t, 1H), 4.91 (dd, 1H), 3.33 (q, 2H), 2.91–2.68 (m, 3H), 2.34 (t, 2H), 2.16–2.10 (m, 1H), 1.97–1.90 (m, 2H), 1.45 (s, 9H). **LC-MS (ESI$^+$):** m/z = 416.2 (M + H)$^+$.

Preparation of4-((2-(2,6-dioxopiperidin-3-yl)-1,3-dioxoisoindolin-4-yl)amino)butanoic acid (Compound 18).

Compound 18 was prepared from **17** (50 mg) using General Procedure B. The deprotection yielded **18** (50 mg) as a pale-yellow viscous liquid. This crude product was used directly in the next step without purification [18].

Preparation of4-((4-(5′-(benzo [d] [1,3] dioxol-5-yl)-2′-oxo-1′,2′-dihydrospiro [piperidine-4,3′-pyrrolo [2,3-*b*] pyridin] -1-yl)-4-oxobutyl)amino)-2-(2,6-dioxopiperidin-3-yl)isoindoline-1,3-dione (PN-II-05).

To a stirred solution of **1** (50 mg, 0.154 mmol) in DMF (0.5 mL) at 0 °C under a nitrogen atmosphere were added **18** (52 mg, 0.154 mmol), HATU (70 mg, 0.184 mmol, 1.2 equiv.), and DIPEA (0.08 mL, 0.462 mmol, 3 equiv.). The reaction mixture was stirred at room temperature

for 1 h and monitored by TLC. After completion, the mixture was diluted with water (3 mL) and extracted with ethyl acetate (3 × 12 mL). The organic layer was washed with brine, dried over sodium sulfate, and concentrated under reduced pressure. Purification was performed twice using GRACE C18 reverse-phase chromatography (12 g, RELEVERIS), eluting with 35–40% acetonitrile/0.05% formic acid in water. The product fractions were lyophilized to afford **PN-II-05** (20 mg, 20%) as a pale yellow solid. **^{1}H NMR** (400 MHz, DMSO-d_6): δ 11.12 (s, 1H), 11.08 (s, 1H), 8.49 (s, 1H), 8.33 (d, 1H), 8.09 (d, 1H), 7.62–7.58 (m, 1H), 7.32 (d, 1H), 7.18 (dd, 2H), 7.01 (dd, 2H), 6.70 (t, 1H), 6.05 (s, 2H), 5.65–5.02 (m, 1H), 3.89–3.73 (m, 4H), 2.91–2.82 (m, 2H), 2.55–2.50 (m, 6H), 2.08–2.07 (m, 1H), 1.87–1.75 (m, 6H). **^{13}C NMR** (400 MHz, DMSO-d_6): δ 180.4, 172.9, 170.2, 170.0, 168.8, 167.3, 154.9, 147.9, 146.7, 146.3, 144.1, 136.2, 132.2, 131.6, 129.9, 129.6, 128.2, 120.0, 117.3, 110.3, 109.0, 108.6, 107.0, 101.1, 48.5, 45.3, 41.6, 36.6, 31.9, 31.4, 30.9, 29.5, 24.3, 22.1. **LC-MS (ESI$^+$):** m/z = 665.2 $(M + H)^+$; **IR:** 1699.2 cm^{-1} (C═O stretching); **Melting range:** 163–166 °C.

Preparation of tert-butyl 3-((2-(2,6-dioxopiperidin-3-yl)-1,3-dioxoisoindolin-4-yl)amino)propanoate (Compound 20).

To a stirred solution of 3-(4-amino-1-oxoisoindolin-2-yl)piperidine-2,6-dione **(19)** (500 mg, 1.93 mmol, 1.0 equiv.) and tert-butyl 2-bromoacetate **(6)** (0.4 mL, 2.12 mmol, 1.1 equiv.) in acetonitrile (5 mL), potassium carbonate (399 mg, 2.89 mmol, 1.5 equiv.) was added at room temperature. The mixture was stirred at 100 °C for 16 h and monitored by TLC and LC-MS. Upon completion, the reaction mixture was cooled, diluted with water (10 mL), and extracted with ethyl acetate (3 × 15 mL). The organic layer was washed with water and brine, dried over sodium sulfate, and concentrated under reduced pressure. The crude product was purified using GRACE silica chromatography (12 g, RELEVERIS), eluting with 30–50% ethyl acetate in petroleum ether, to afford **20** (600 mg, 83%) as a pale yellow foamy solid. **LC-MS (ESI$^+$):** m/z = 318.1 $(M + H–tBu)^+$.

Preparation of(2-(2,6-dioxopiperidin-3-yl)-1-oxoisoindolin-4-yl)glycine (Compound 21).

Compound 21 was prepared from **20** (60 mg) using General Procedure B, affording crude **(**2-(2,6-dioxopiperidin-3-yl)-1-oxoisoindolin-4-yl)glycine **(21)** (60 mg) as a pale-yellow viscous liquid. This product was used in the next step without purification [19].

Preparation of3-(4-((2-(5′-(benzo [d] [1,3] dioxol-5-yl)-2′-oxo-1′,2′-dihydrospiro [piperidine-4,3′-pyrrolo [2,3-*b*] pyridin] -1-yl)-2-oxoethyl)amino)-1-oxoisoindolin-2-yl)piperidine-2,6-dione (PN-II-06).

To a stirred solution of **1** (50 mg, 0.154 mmol) in DMF (0.5 mL) at 0 °C under a nitrogen atmosphere were added **21** (60 mg, 0.184 mmol, 1.2 equiv.), HATU (86 mg, 0.225 mmol, 1.5 equiv.), and DIPEA (0.078 mL, 0.462 mmol, 3 equiv.). The reaction mixture was stirred at room temperature for 2 h and monitored by TLC. After completion, the mixture was diluted with water (5 mL) and extracted with ethyl acetate (3 × 10 mL). The organic layer was washed with brine (2 × 10 mL), dried over sodium sulfate, and concentrated under reduced pressure. Purification was performed twice using GRACE reverse-phase chromatography (12 g C18, RELEVERIS), eluting with 30–40% acetonitrile/0.05% formic acid in water. The purified fractions were lyophilized to afford **PN-II-06** (25 mg, 25%) as a pale yellow solid. **^{1}H NMR** (400 MHz, DMSO-d_6): δ 11.11 (s, 1H), 8.34 (s, 1H), 8.13 (d, 1H), 7.34 (s, 1H), 7.21–7.17 (m, 2H), 6.99–6.92 (m, 2H), 6.80 (d, 1H), 6.08 (s, 2H), 5.47 (s, 2H), 5.29 (dd, 1H), 4.59 (dd, 2H), 4.23 (dd, 1H), 4.04 (dd, 1H), 3.92–3.77 (m, 4H), 3.18–3.04 (m, 1H), 2.85 (d, 1H), 2.37–2.28 (m, 1H), 2.16 (bs, 1H), 1.87–1.77 (m, 4H).

^{13}C NMR (400 MHz, DMSO-d_6): δ 180.1, 171.5, 170.4, 169.0, 164.3, 154.9, 147.9, 146.7, 146.7, 144.1, 143.6, 132.1, 131.5, 129.9, 129.6, 128.0, 125.5, 120.1, 116.4, 110.4, 108.6, 107.1, 101.1, 51.8, 45.3, 41.0, 37.1, 31.8, 31.3, 22.1. **LC-MS (ESI$^+$):** m/z = 623.2 $(M + H)^+$; **IR:** 1681.9 cm^{-1} (C═O stretching); **Melting range:** 208–210 °C.

4.3. Computational modeling of PROTAC–target–E3 ligase complexes

4.3.1. Data retrieval and protein preparation

Relevant PDB structures of BTK and E3 ligases were retrieved from the Protein Data Bank. Specifically, BTK co-crystallized with Ibrutinib (PDB ID: 5P9J) and the thalidomide-binding E3 ligase CRBN (PDB ID: 4TZ4) were selected for modeling [20,21]. Structures lacking ligand bound conformations such as the androgen receptor or PROTACs lacking a defined E3 ligase (e.g., IAP-based systems) were excluded due to modeling limitations.

The mutant BTK structure (C481S) was generated using UCSF Chimera [22]. The Cys481 residue was substituted with serine using the Rotamers tool, which allows amino acid changes while optimizing side-chain orientation. The rotamer with the best steric fit and minimal clashes was selected. After the mutation, the structure was energy-minimized using the AMBER force field to relax any local strain caused by the substitution. The minimized model was then visually inspected to confirm overall structural integrity and correct geometry of the active site. The final mutant structure was saved in PDB format and used for further docking studies.

Protein preparation followed the PROTAC Model protocol. Nonstandard atoms were corrected, and structures were processed in UCSF Chimera 2020 [22], involving bond order assignment, water removal, hydrogen addition, side-chain completion, and energy minimization using the AMBER 2005 force field [23]. E3 ligands were prepared separately using ACD/Labs steepest descent (1000 steps) and the AMBER ff4 force field. Binding sites were defined according to the co-crystallized ligand.

4.3.2. Docking of ternary complexes

Ternary complex formation was modeled using the HDOCK protocol [24,25]. The receptor protein remained fixed while the ligand was sampled in 3D space using 1.2 Å translational steps and 15° rotational increments. Fast Fourier Transform (FFT) was employed to enhance sampling efficiency. Shape-based scoring functions were used to evaluate configurations during each rotation, and the top 10 translational poses were re-ranked using an internal scoring algorithm.

A total of 4382 uniformly distributed rotations in Euler space were sampled. The highest-scoring binding mode for each rotation was selected. Redundant configurations were clustered based on RMSD to identify representative poses [26].

4.4. Biological evaluation of PROTAC compounds

4.4.1. Cell lines

Cell lines were obtained from ATCC (Middlesex, UK) and DSMZ (Braunschweig, Germany) and maintained at 37 °C in a humidified incubator with 5% CO_2. Cells were grown in recommended media supplemented with 10% fetal calf serum, streptomycin (100 mg/mL), penicillin (100 U/mL), 2 mM glutamine, 1 mM sodium bicarbonate, 1 mM sodium citrate, and 20 mM HEPES. Mycoplasma testing was performed biweekly or monthly [27,28]. All BTK-expressing cancer cell lines used in this study, including RAMOS, harbor wild-type BTK and do not carry resistance-associated mutations such as C481S.

4.4.2. Cytotoxicity assay

Cytotoxicity was assessed using an MTS assay optimized for drug screening. IC_{50} values were determined as described previously [29].

4.4.3. Kinase inhibition assay

Kinase inhibition was evaluated using recombinant ITK and BTK proteins (ITK: BPS Biosciences, Cat. #78429; BTK: Promega, Cat. #V2941) [10]. Enzymes were diluted to 5 ng/μL in assay buffer; the BTK buffer was supplemented with 50 μM DTT and 2 mM $MnCl_2$. Compounds were diluted in 10% DMSO (final concentration: 0–10 μM). Ibrutinib (100 nM) served as a positive control. Reactions were assembled in 384-

well plates and incubated before assessing activity with the ADP-Glo™ Kinase Assay (Promega, Cat. #V9101). Luminescence was measured using a Tecan Infinite 200 PRO reader. Data were normalized to DMSO (100% activity) and no-enzyme (0%) controls. IC_{50} values were calculated by nonlinear regression using either a three- or four-parameter logistic model in GraphPad Prism (GraphPad Software, Boston, MA, USA).

4.4.4. BTK degradation assay and Western blotting

RAMOS cells were seeded in 6-well plates and treated with PN-II-05 (0–10 μM) for 24 h. DMSO-treated cells served as vehicle controls (final DMSO concentration < 0.5%). Following treatment, cells were washed with PBS and lysed in RIPA buffer (Thermo Fisher, Cat. #89901) supplemented with protease and phosphatase inhibitors (Roche, Cat. #04693116001 and #04906837001). Lysates were sonicated at 4 °C (Qsonica Cup Horn sonicator, 25% amplitude, 1 min total, 5 s off/10 s on) and centrifuged at 13,000 ×*g* for 30 min. Protein concentrations in the supernatants were quantified using the BCA assay (Thermo Fisher, Cat. #23223, #23224).

Equal amounts of protein (30 μg) were resolved by 10% SDS-PAGE and transferred onto nitrocellulose membranes (Bio-Rad, Cat. #170–4270) using the Trans-Blot Turbo system. Membranes were blocked in 5% BSA/TBST, then incubated with primary antibodies against BTK (Cell Signaling, Cat. #3533S) and GAPDH (Cell Signaling, Cat. #2118S), followed by Alexa Fluor 488-conjugated secondary antibodies (Invitrogen, Cat. #A21202 and #A11034). Blots were imaged using a ChemiDoc MP imaging system (Bio-Rad, California, United States), and densitometry was performed using the ImageJ software (RRID: SCR_003070).

4.4.5. Blot quantification and analysis

Band intensities were quantified using NIH ImageJ software and normalized to GAPDH as a loading control. Percent degradation was calculated relative to DMSO-treated controls and fitted using a four-parameter logistic model in GraphPad Prism to determine DC_{50} and Dmax values, as previously described [10]. Statistical significance was set at $P < 0.05$.

CRediT authorship contribution statement

Naveen Kumar Rampeesa: Writing – original draft, Methodology, Investigation, Formal analysis. **Rambabu Gundla:** Writing – review & editing, Supervision, Project administration. **Soňa Gurská:** Investigation, Formal analysis, Data curation. **Sabitha Yadam:** Validation, Methodology. **Sudhakar Tangallapalli:** Visualization, Formal analysis. **Sreenivasa Reddy Anugu:** Resources, Conceptualization. **Juan Bautista De Sanctis:** Visualization, Methodology. **Petr Džubák:** Resources, Methodology. **Marián Hajdúch:** Writing – review & editing, Conceptualization. **Naresh Kumar Katari:** Data curation, Conceptualization. **Viswanath Das:** Writing – review & editing, Investigation, Funding acquisition, Conceptualization. **Sreekantha Babu Jonnalagadda:** Writing – review & editing, Funding acquisition.

Declaration of competing interest

The authors declare the following financial interests/personal relationships which may be considered as potential competing interests: Naveen Kumar Rampeesa, Rambabu Gundla, Gopal Mudasani, Sreenivasa Anugu, and Viswanath Das are listed as inventors on a published patent application titled “Azaspirooxindolinone based PROTAC compounds to target ITK and BTK kinases”, Indian Patent Application No. 202441059537 A. The remaining authors declare no competing interests.

Acknowledgements

Dr. Rambabu Gundla acknowledges financial support from DBT-BIRAC (BT/AIR01566/PACE-27/22) and GITAM for providing necessary facilities. RN and RG thank Aragen Lifesciences Pvt. Ltd., Hyderabad, India, for computational support and for synthesizing and characterizing all compounds using NMR, LC-MS, and FT-IR. The biological part of the study was supported in part by infrastructural projects CZ-OPENSCREEN (LM2023052), EATRIS-CZ (LM2023053), and the Czech biobank network BBMRI (LM2023033), as well as by the National Institute for Cancer Research (EXCELES, LX22NPO5102), the National Institute for Neurological Research (EXCELES, LX22NPO5107) funded by the European Union – Next Generation EU through the Ministry of Education, Youth and Sports of the Czech Republic, the Technology Agency of the Czech Republic (project TN02000109, Personalized Medicine: From Translational Research into Biomedical Applications, within the National Centers of Competence Program), and the SALVAGE project (CZ.02.01.01/00/22_008/0004644) supported by OP JAK, co-financed by the European Union and the State Budget.

Appendix A. Supplementary data

Supplementary data to this article can be found online at https://doi.org/10.1016/j.rechem.2026.103145.

Data availability

No data was used for the research described in the article.

References

[1] A. Wolska-Washer, P. Smolewski, Targeting protein degradation pathways in tumors: focusing on their role in hematological malignancies, Cancers 14 (15) (2022) 3778, https://doi.org/10.3390/cancers14153778.
[2] Ghui Sun, Xin Luo, Zimo Yang, Lixia Chen Wenxinglv, Hua Li, Yu Rao, Developing potent BTK ^{c481s} PROTACs for ibrutinib-resistant malignant lymphoma, Chin. Chem. Lett. 34 (2023). Issue 6–107924.
[3] A. Alu, H. Lei, X. Han, et al., BTK inhibitors in the treatment of hematological malignancies and inflammatory diseases: mechanisms and clinical studies, J. Hematol. Oncol. 15 (2022) 138, https://doi.org/10.1186/s13045-022-01353-w.
[4] S. Liu, Y. Da, F. Wang, et al., Targeted selective degradation of Bruton's tyrosine kinase by PROTACs, Med. Chem. Res. 29 (2020) 802–808, https://doi.org/10.1007/s00044-020-02526-3.
[5] Xiu-Juan Liu, XU-Liu, Xiao-Jing Pang, Xin-Ying Yuan, Guang-XI-Yu, yin-Ru-Li, Yang-feng Guan, Yan-Bing Zhang, Jian song, Qiu-Rong Zhang, Sai-Yang Zhang, Progress in the development of small molecular inhibitors of the Bruton'sTyrosin kinase (BTK) as a promising cancer therapy, Bioorg. Med. Chem. 47 (2021) 116358.
[6] HarshitaSachdeva, Jaya Mathur, Anjali Guleria, Indole derivatives as potential anticancer agents: a review, J. Chil. Chem. Soc. 65 (2020).
[7] Dilan Konyar, Cenk a.Andac, ErdemBuyukbingol, Design, synthesis and cytotoxic activity of spiro(oxindole-3-3-pyrrolidine) derivatives, Lett. Drug Des. Discov. 15 (2018).
[8] A.K. Gupta, M. Bharadwaj, A. Kumar, et al., Spiro-oxindoles as a promising class of small molecule inhibitors of p53–MDM2 interaction useful in targeted cancer therapy, Top CurrChem (Z) 375 (2017) 3, https://doi.org/10.1007/s41061-016-0089-0.
[9] Liangkun Ji, Ying Zhou, Qiuyan Yu, Yaxuan Fang, Yongjiunjiang, Yunhui Zhao, chuntao yuan, wenlinxie, Synthesis and anticancer activity of new spirooxindoles incorporating[1,2,4]triazolo[3,4-b][1,3,4]thiadiazine moiety, J. Mol. Struct. 1227 (2021) 129406.
[10] Naveen Kumar Rampeesa, Rambabu Gundla, Gopal Muddasami, Sudhakar, Sreenivasa Reddy Anugu, Soňa Gurská, Juan Bautista De Sanctis, Petr Džubák, Marián Hajdúch, Viswanth Das, Novel azaspirooxindolinone-based PROTACs for selective BTK degradation and enhanced anticancer activity, Bioorg. Chem. 157 (2025) 108316.
[11] W. Guo, R. Liu, Y. Ono, A.H. Ma, A. Martinez, E. Sanchez, Y. Wang, W. Huang, A. Mazloom, J. Li, J. Ning, E. Maverakis, K.S. Lam, H.J. Kung, Molecular characteristics of CTA056, a novel interleukin-2-inducible T-cell kinase inhibitor that selectively targets malignant T cells and modulates oncomirs, MolPharmacol 82 (5) (2012) 938–947, https://doi.org/10.1124/mol.112.079889.
[12] H. Wu, W. Wang, F. Liu, E.L. Weisberg, B. Tian, Y. Chen, B. Li, A. Wang, B. Wang, Z. Zhao, D.W. McMillin, C. Hu, H. Li, J. Wang, Y. Liang, S.J. Buhrlage, J. Liang, J. Liu, G. Yang, J.R. Brown, S.P. Treon, C.S. Mitsiades, J.D. Griffin, Q. Liu, N. S. Gray, Discovery of a potent, covalent BTK inhibitor for B-cell lymphoma, ACS Chem. Biol. 16 (5) (2014) 1086–1091, https://doi.org/10.1021/cb4008524.

[13] Shaodong Liu, Da Yang, Feng Wang, Renjie Yan, Yongzhi Shu, Lin Pei, Jun Lin, Targeted selective degradation of Bruton's tyrosine kinase by PROTACs, Med. Chem. Res. (2023), https://doi.org/10.1007/s00044-020-02526-3.
[14] G. Mudasani, K. Paidikondala, R. Gundla, S. Joseph Maddirala, V. Das, Synthesis and biological evaluation of 5′-arylspiro[piperidine-4,3′-pyrrolo-[2,3-b]pyridin] analogues, ChemistrySelect 6 (2021) 3378–3381, https://doi.org/10.1002/slct.202004719.
[15] J. Qi, S. Armstrong, L. Wu, Compounds, compositions, and methods for protein degradation, WO2020264172A1. https://patents.google.com/patent/WO2020264172A1/en?oq=+WO2020%2f264172, 2020 accessed June 7, 2024.
[16] Pearlie BURNETTENicholas, J. LawrenceHarshani, Lawrence, Preparation of dimeric compounds as immuno-modulators against cereblon-based mechanisms, WO2020014489 A2. https://patents.google.com/patent/WO2020014489A2/en?oq=WO2020014489, 2020.
[17] AnandDivakaranCole, R. ScholtzHudaZahidWenweiLinElizabeth, C. GriffithRichard, E. LeeTaoshengChenDaniel, A. Harki William, C.K. Pomerantz, Development of an N-terminal BRD4 bromodomain-targeted degrader, ACS Med. Chem. Lett. 13 (10) (2022) 1621–1627, https://doi.org/10.1021/acsmedchemlett.2c00300.
[18] Daniel W. Robbins, Ge Peng, Jeffrey Mihalic, Arthur T. Sands, Bifunctional compounds for degrading BTK via ubiquitin proteasome pathway, WO2021091575A1. https://patents.google.com/patent/WO2021091575A1/en?oq=WO2021091575+A1, 2021.
[19] Kandaswamy Vijayan, et al., System of bead-bound DNA barcodes for screening chemical compounds for their biological activity, US20230065224 A1. https://www.freepatentsonline.com/result.html?sort=relevance&srch=top&query_txt=US20230065224+A1&submit=&patents_us=on&patents_other=on, 2023.
[20] A.T. Bender, A. Gardberg, A. Pereira, T. Johnson, Y. Wu, R. Grenningloh, J. Head, J. Morandi, F. Haselmayer, P. Liu-Bujalski, Ability of Bruton's tyrosine kinase inhibitors to sequester Y551 and prevent phosphorylation determines potency for inhibition of fc receptor but not B-cell receptor signaling, Mol. Pharmacol. 91 (2017) 208–219.34.
[21] P.P. Chamberlain, M. Wang, S. Delker, G. Carmel, K. Miller, A. Lopez-Girona, B. Pagarigan, B. Leon, K. Rychak, L. Corral, A. Lopez-Girona, Y. Ren, M. Wang, M. Riley, S. Delker, T. Ito, A. Hideki, T. Mori, H. Handa., T. Hakoshima, T. O. Daniel, K. Miller, B.E. Cathers, G. Carmel, Structural Pagarigan, Basis for Responsiveness to Thalidomide-Analog Drugs Defined by the Crystal Structure of the Human Cereblon:DDB1:Lenalidomide Complex, 2014.
[22] F. Pettersen, T.D. Goddard, C.C. Huang, S. Couch, D.M. Greenblatt, E.C. Meng, T. E. Ferrin, UCSF chimera visualization system for exploratory research and analysisJournal of Computational Chemistry 25 (13) (2004) 1605–1612.
[23] Jennifer Loschwitz, Anna Jackering, Monika Keutmann, Maryam Olagunju, Olujide O. OLubiyi, Birgit Strodel, Dataset of Amber force field parameters of drugs, natural products, and steroids for stimulations using GROMACS, Data in Brief 35 (2021) 106948.
[24] H. Li, E. Huang, Y. Zhang, S.Y. Huang, Y. Xiao, HDOCK update for modeling protein-RNA/DNA complex structures, Protein Sci. 11 (2022) e4441, https://doi.org/10.1002/pro.4441.
[25] Yumeng Yan, Di Zhang, Pei Zhou, Botong Li, Sheng-You Huang, HDOCK: a web server for protein–protein and protein–DNA/RNA docking based on a hybrid strategy, Nucleic Acids Res. 45 (W1) (2017) W365–W373, https://doi.org/10.1093/nar/gkx407.
[26] Gaoqiweng, Xuanyan Cai, Dongsheng Cao, Hongyan Du, Chao shen, Yafeng Deng, Qiaojun He, Bo Yang, Dan Li, Ting junHou, PROTAC-DB 2.0: an updated database of PROTACs, Nucleic Acids Res. 51 (2023) D1367–D1372, https://doi.org/10.1093/nar/gkac946. Database issue.
[27] R. Buriánová, J. Kotulová, Detection of mycoplasma contamination in cell lines by PCR (Chapter 5), in: J. Drábek, V. Das, P. Dzubak, Josef Strovnal, J. Bouchal, M. Hajduch, K. Koberna, A. Ligasová, M. Mistrik, J. De Sanctis (Eds.), Laboratory Techniques in Cellular and Molecular Medicine, 1st ed., Palacký University Olomouc, Olomouc, 2022, pp. 37–42, https://doi.org/10.5507/lf.22.24460499.
[28] J. Stránská, STR profiling for cell line authentication (Chapter 4), in: J. Drábek, V. Das, P. Dzubak, Josef Strovnal, J. Bouchal, M. Hajduch, K. Koberna, A. Ligasová, M. Mistrik, J. De Sanctis (Eds.), Laboratory Techniques in Cellular and Molecular Medicine, 1st ed., Palacký University Olomouc, Olomouc, 2022, pp. 29–36, https://doi.org/10.5507/lf.22.24460499.
[29] S. Nisitani, R.M. Kato, D.J. Rawlings, O.N. Witte, M.I. Wahl, In situ detection of activated Bruton's tyrosine kinase in the Ig signaling complex by phospho peptide specific monoclonal antibodies, Proc. Natl. Acad. Sci. 96 (1999) 2221–2226, https://doi.org/10.1073/pnas.96.5.2221.